DOI: 10.48011/sbse.v1i1.2290

# Analysis of High Impedance Faults Current Using Fourier, Wavelet and Stockwell Transforms

**Gabriela N. Lopes, Luiz H. P. C. Trondoli, José Carlos M. Vieira**

*Universidade de São Paulo (USP) - Escola de Engenharia de São Carlos (EESC), São Carlos - SP. (emails: gabrielanuneslopes@usp.br, luiz.trondoli@usp.br, jcarlos@sc.usp.br)*

**Abstract:** Detection of high impedance faults (HIFs) in distribution systems is a challenging task, which has attracted the interest of the researchers for decades. The HIF current random behavior and its low magnitude cause difficulties for a reliable detection by traditional protection methods. Therefore, the hazards for grid devices, people and animals safety, associated with HIFs, motivate the research of new detection techniques. However, there is no fully efficient solution for this problem. In this context, this paper aimed to characterize HIFs by a set of real measurements considering different type of soils employing Fourier (FT), Wavelet (WT) and Stockwell Transforms (ST). The measurements were performed at the fault spot in a medium voltage test field specially built for this purpose. The idea is to highlight key characteristics of the HIF current waveforms pointed out by each of transform and assess which ones can be used as a promising tool for HIF detection. The results showed that the HIF current can be characterized by the interharmonic behavior during the fault, extracted by FT and by the high degree of energy variations at specific decomposition levels of WT and ST.

**Resumo**: A detecção de Faltas de Alta Impedância (FAIs) em sistemas de distribuição é uma tarefa árdua que atrai o interesse de pesquisadores por décadas. O comportamento aleatório da corrente de FAI e a sua baixa magnitude causam dificuldades para uma detecção confiável pelos métodos tradicionais. Portanto, os perigos relacionados a dispositivos da rede, pessoas e animais, associados com FAIs, motivam a pesquisa de novas técnicas de detecção. No entanto, não há solução totalmente eficiente para este problema. Neste contexto, este artigo focou em caracterizar FAIs por um conjunto de medições considerando diferentes tipos de solo empregando as transformadas de Fourier (TF), Wavelet (TW) e Stockwell (TS). As medições foram realizadas no ponto de falta de uma rede de teste de média tensão especialmente construída para este propósito. A ideia é evidenciar as características chave da forma de onda de corrente de FAIs apontadas por cada transformada e avaliar quais delas podem ser utilizadas como uma técnica promissora de detecção de FAIs. Os resultados mostraram que a corrente de FAI pode ser caracterizada pelo comportamento dos interharmônicos durante a falta, extraído pela TF, e pelo alto nível de variação de energia em níveis de decomposição específicos da TW e TS.

*Keywords:* Distribution Systems; Fourier transform; High Impedance Faults; Stockwell transform; Wavelet transform.

*Palavras-chaves:* Sistemas de distribuição; Transformada de Fourier; Faltas de alta impedância; Transformada de Stockwell; Transformada Wavelet.

## 1. INTRODUCTION

Power distribution systems (PDS) are frequently subjected to High Impedance Faults (HIFs) and to the dangerous effects that this disturbance can cause, if not detected and extinguished timely. HIFs are caused by the contact of energized conductors with high impedance surfaces, such as vegetation and soil. The HIF current is no larger than the load current, therefore it cannot be detected by traditional overcurrent protection.

Even with the manufacturers efforts to develop efficient protection devices for detecting such disturbance, commercial relays are able to identify only from 50 % to 60 % of HIFs (Nam, Park, Kang, and Kim, 2001). Therefore, developing means of providing an understanding of this phenomenon are highly required by the power industry. In this context, most of the papers found in literature proposed and/or assessed HIF detection methods based on the conductor rupture with its posterior drop on the soil (Santos, Lopes, Brito, and Souza, 2017).

Traditionally, the detection of HIFs is carried out by the features extracted from the fault current and voltage measurements, employing either frequency or time-domain techniques. Therefore, HIFs can be divided into two classes: soil contact (Carvalho et al., 2015) and vegetation contact (Gomes et al., 2018). In this context, a remarkable characteristic is the electric arc, which causes asymmetry, build-up and shoulder on the HIF current waveform (Gomes et al., 2018). Recently, interharmonic-based methods have emerged as a promising approach to detect HIF (Carvalho et al., 2015). In the same way, Discrete Wavelet Transform (DWT) was employed in Santos et al. (2017) to analyze low and high frequency induced components in the voltage during the occurrence of HIFs. In addition, the use of the Stockwell Transform (ST) has emerged as another potential tool for detecting HIFs, as claimed by Mohamad and Abidin (2012) and Routray et al. (2015).

Besides those three techniques, the forthcoming evolution of power networks to smart grids creates opportunities for new technologies to be implemented for that purpose (Milioudis, Andreou, and Labridis, 2012). For instance, in Milioudis et al. (2012), Power Line Communication (PLC) is used for detection and location of HIFs. Additionally, algorithms have also been developed to detect HIFs based on the identification of nonlinear voltage–current characteristic profiles as proposed in Wang et al. (2018), which could also be popularized in the

applications of relay protection, harmonic source location and early fault alarming in smart grid.

Therefore, as different signal processing techniques presented satisfactory results, comparing their performance at analyzing HIFs current waveforms can provide useful insights for developing new and improving existing HIFs detection methods. In this context, this paper aims to characterize HIF currents according to the previously-mentioned transforms: Fourier, wavelet and Stockwell, so that advantages and disadvantages of each one are highlighted. A set of actual HIFs current waveforms, obtained from a distribution utility, was used in the studies carried out in this work.

These experiments comprised dropping energized conductors on the ground considering different types of soil: sand, gravel, grass and clay. The results showed that HIF signals were satisfactorily characterized by Fourier, wavelet and Stockwell transforms, thus, from each of them, key factors can be used for identifying HIFs efficiently.

## 2. THEORETICAL BACKGROUND

### *2.1 Wavelet Transform (WT)*

According to Belka and Michalik (2004), the HIF current waveforms present discontinuities on zero crossing regions, caused by the extinction and re-ignition of the electric arc, resulting in energy variation. This behavior is suitable for wavelet transform-based methods, because of their good capability to detect those sudden changes. Thus, it is possible to identify those energy variations by analyzing the coefficients of the wavelet transform.

The WT *C(a, b)* of a signal *f(t)* can be calculated by (1) with a mother-wavelet $\psi(t)$. In this paper, a mother-wavelet *Haar* in continuous time was used, which is described by (2), (3) and (4) (Nason et al., 2001).

$$C(a,b) = \int_{-\infty}^{+\infty} f(t)\,\psi(t)\,dt \tag{1}$$

$$\psi(t) = \frac{1}{\sqrt{2}},\ if\ t\ \epsilon\ (0, \frac{1}{2}) \tag{2}$$

$$\psi(t) = \frac{-1}{\sqrt{2}}\ , if\ t\ \epsilon\ (\frac{1}{2}, 1) \tag{3}$$

$$\psi(t) = 0\ \ for\ any\ other\ value\ of\ t \tag{4}$$

In the one-signal WT, the details and approximations are derived in a hierarchical and multiresolution way with a scaling factor of 2 (Belka and Michalik, 2004).

### *2.2 Fourier Transform (FT)*

The Fourier transform extracts the frequency content of a signal and it is employed in this paper to provide the frequencies multiples of 60 Hz and interharmonic signature of HIF current waveform. At each current waveform cycle, (5) was applied, as shows:

$$X[n] = \sum_{k=0}^{N-1} x[k] e^{\frac{-j\pi nk}{N}} \tag{5}$$

where *n= 0, 1, 2, ..., N-1*, *X[n]* is the signal in the frequency domain, *x[k]* is the signal in time domain and *N* is the number samples.

In order to observe certain signal frequencies, the size, and consequently the number of samples in each window, can be changed, thus modifying the frequency resolution $\Delta\ f$ of the signal with a sampling frequency $f_s$, as shown below:

$$\Delta f = \frac{f_s}{N} \tag{6}$$

Interharmonics are commonly found in HIF current waveforms, because they are associated with the random length variation of the electric arc during fault situations. In this condition, the larger the amplitude of the variation, the larger the number of interhamonic frequencies (Carvalho et al., 2015).

### *2.3 Stockwell Transform (ST)*

The ST can be considered as the extension of the Fast Fourier transform, which is given by (7):

$$S(\tau, f) = \int_{-\infty}^{+\infty} h(t)\omega(t-\tau, f) e^{-j2\pi ft} dt \tag{7}$$

where $\tau$ is the time spectral localization, $f$ means the Fourier frequency and $h(t)$ is the signal.

However, the ST analyzes the signal from a Gaussian window $\omega(t, f)$, described as:

$$\omega(t, f) = \frac{1}{\sigma(f)\sqrt{2\pi}} e^{\frac{-t^2}{2\sigma(f)^2}} dt \tag{8}$$

with a standard deviation $\sigma(f)$ inversely proportional to the signal frequency as shown:

$$\sigma(f) = \frac{1}{|f|}. \tag{9}$$

Thus, by replacing (8) and (9) into (7), the continuous ST of a signal *h(t)* can be calculated by (10), as shows:

$$S(\tau, f) = \int_{-\infty}^{+\infty} h(t) \frac{|f|}{\sqrt{2\pi}} e^{-\frac{(\tau-t)^2 f^2}{2}} e^{-j2\pi ft} dt. \tag{10}$$

In this way, the Discrete Stockwell Transform was used, and for a discrete series H[kT], it can be calculated as (11) (Stockwell et al., 1996):

$$S[jT, \frac{n}{NT}] = \sum_{m=0}^{N-1} H[\frac{m+n}{NT}] e^{-\frac{2\pi^2 m^2}{n^2}} e^{-\frac{i2\pi mp}{N}} \quad , n \neq 0 \tag{11}$$

where *p*, *m* and *n*= 0, 1, ..., *N*-1, where *n* represents the harmonic orders.

The ST is a multiresolution spectral analysis technique, where the standard deviation is an inverse function of the frequency, reducing the dimension of the transform (Samantaray et al., 2008), and provides the amplitude and phase of the harmonic orders at each signal sample. This way, in this paper the HIF current waveform was broken down into the desired harmonic orders during the fault period.

### *2.4 Energy*

In this paper, the HIF current is characterized by the energy spectrum (E), calculated for all coefficients of the transforms, as given by (12),

$$E = \sum_{n=t_1}^{t_2} |x(n)|^2 \tag{12}$$

in which *x(n)* represents the value of each sample, $t_1$ represents the first sample of the window and $t_2$ the last. For all transforms the signal will be traversed by a sliding window and the energy of the resolution levels calculated.

## 3. RESULTS

This section presents the results of the three transforms, developed in Matlab, on the HIFs current for sandy, gravel, grass and clay soils. The HIF waveforms were obtained by the authors of Carvalho et al. (2015). They were measured at the fault location in a medium voltage (13.8 kV) test field in Brazil, specially

built for this purpose. The data were measured dropping only one phase of energized conductors on the ground, acquired with 16 samples per cycle. All data presented in this section contains only the current recorded at the fault location after the conductor touches the ground, that is, only during the high impedance fault.

### *3.1 HIF current waveforms*

The HIF current waveforms obtained experimentally for the soils are shown at Fig. 1. The differences among HIF currents are due to the random behavior of the electric arc, soil type and its characteristics, such as humidity and resistivity. It is noted that in all cases there was extinction (current equal to 0) and subsequent re-ignition of the electric arc. Also, in these cases, the fault current was around 10 A, lower than the load current in several distribution circuits, which demonstrates the difficulty of identifying this type of fault by conventional protection.

### *3.2 Analysis by Fourier Transform (FT)*

For all the current measurements, a 12-cycle window was used, as well as in Carvalho et al. (2015), to reduce spread spectrum superposition, resulting in a frequency resolution of 5 Hz, and allowing the visualization of the interharmonic frequencies of the signals. This window was shifted cycle by cycle until the end of the fault signal. The values of the energies of the harmonics and interharmonics in the windows were sampled in decibels (dB) to facilitate the visualization and comparison. This was done because the energy values for 60 Hz are much higher than the energy of all other frequencies. As the data were acquired with 16 samples per cycle, it is possible to visualize up to the eighth harmonic order, that is, 480 Hz, according to the Nyquist theorem. The figures presented in this section will be in matrix format, in which the left axis represents all signal frequencies, from 0 to 480 Hz with a frequency resolution of 5 Hz. For each window calculated by FT over time, there is color scale for the energy amplitude at each frequency. The dark-red color means large energy value, whereas light colors imply on small energy.

The frequency content of the HIF current for sandy soil is presented in Fig. 2. During the intermittent time, where there is no fault current present, the energy amplitude, in dB, tends to a very low value. During the presence of the electric arc, which causes harmonic distortion to the waveforms, it is possible to identify energy growth in all frequencies analyzed, with values higher than -200 dB. Another characteristic identified is the highest energy value in the integer multiple frequencies of 60 Hz (the harmonic orders).

For gravel, the frequency content is presented in Fig. 3. In this case, after the establishment of the arc, shortly before 6 seconds of fault, the presence of the interharmonics is noticed. Since the signal, shown in Fig. 1, presents modulation there must be interharmonics in the signal, as depicted in Carvalho et al. (2015). In this soil, the energies of the frequencies multiple of 60 Hz were maintained with higher values than the interharmonic frequencies, mainly at 60, 180 and 240 Hz.

When analyzing the HIF current for grass (Fig. 4), similarly to sandy soil and gravel, there is a high growth of the interharmonics energy amplitude throughout the arc duration.

At last, Fig. 5 presents the frequency spectrum of HIF current for clay. The analysis by FT resulted in similar behavior in comparison with sand and gravel.

Thus, the FT shows that HIF has a presence of the harmonic orders. It can be noticed that HIF interharmonics are very relevant, but the ones near the harmonic orders needs further investigation to affirm its genuineness, since the aliasing effect can produce false interharmonics results, as the ones found in Carvalho et al. (2015).

### *3.3 Analysis by the Stockwell Transform (ST)*

The analysis in this section were carried out by calculating the energy of each harmonic order obtained by the ST, from the fundamental until the $8^{th}$ harmonic order. The energy was calculated as in (12), and the results are presented from Fig. 6 to Fig. 9.

For each harmonic order the energy amplitude during the HIF depends on the soil type characteristic. For all soil types, the fundamental order presented higher amplitude than the other harmonic orders. Despite of that, for sand, gravel and clay, the $3^{rd}$ and $4^{th}$ harmonic orders presented higher energy amplitude than the other orders. For grass, the $2^{nd}$ order had the highest energy amplitude during the arc, followed by $3^{rd}$ and $4^{th}$ harmonic orders.

A noticeable characteristic for every soil types is that the energy variation between cycles can be noticed for all harmonic orders.

### *3.4 Analysis by Wavelet Transform (WT)*

In order to calculate the energy of the HIF current waveform by WT, the frequency has been split in four approximation levels (low frequencies), which are the four graphics on the left side of the figures, and four details levels (high frequencies), which are the four graphics on the right side, and for each of these levels the energy value was calculated at each cycle. The results are presented from Fig. 10 to Fig. 13.

Just as ST, the WT shows the increase of the energy value during arc time with greater amplitudes in the first resolutions of approximations and details in all soil types. All resolution levels could characterize the fault signals, however, it is important to note that the way each resolution presents its results depends on the signal sampling frequency, since there is a down sampling by a factor of 2 at each level of WT resolution. In addition, in all resolutions there is variation of the energy value between the cycles, which can also be used as signal characterization.

## 4. DISCUSSION

The FT study showed that there are interharmonics in all HIF signals analyzed. It is noticeable that harmonics and interharmonics were present in all signals, with the prevalence of certain frequencies, showing that FT can be used to characterize HIFs properly. In addition, it is possible to observe that, since the HIF signal presents great variation over time, consequently there will be a change in the energy value in of each harmonic frequency. Fig. 14 shows the energy variation between cycles, in decibels, at all frequencies during the HIF on sandy soil calculated by the FT.

The ST showed that the energy magnitude variation between cycles occurs only during the electric arc presence. For different types of soil, certain harmonic orders prevailed, such as $3^{rd}$ and $4^{th}$. Even harmonic orders are present in HIF signals due to asymmetry, while the $3^{rd}$, for example, is provided by arc ignition. Both effects are caused by the electric arc.

Therefore, the energy variation can be useful for developing a HIF detection method. For showing these results, Table I presents the average energy amplitude variation between cycles for all harmonic orders analyzed by ST only during the arc period for each type of soil.

When applying the WT, similar results of the ST related to the energy variation between cycles were obtained. Table 2 presents

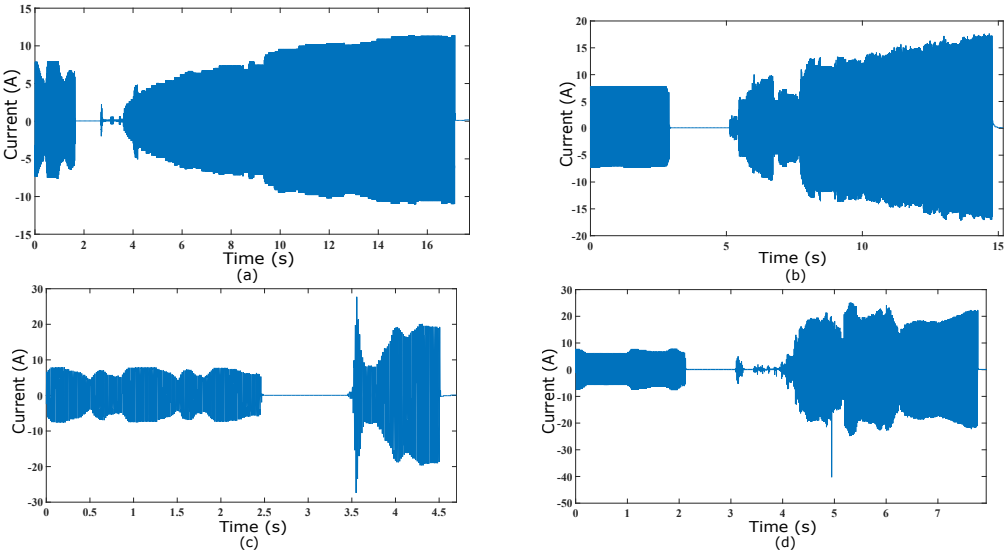


Fig. 1. HIF current waveform registered in the field with the conductor touching soils mainly composed by (a) sand, (b) gravel, (c) grass and, (d) clay.

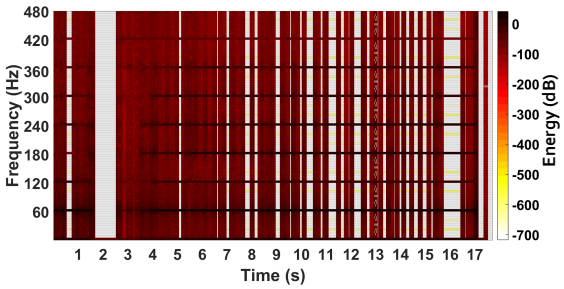


Fig. 2. Current frequencies energy for sandy soil by FT.

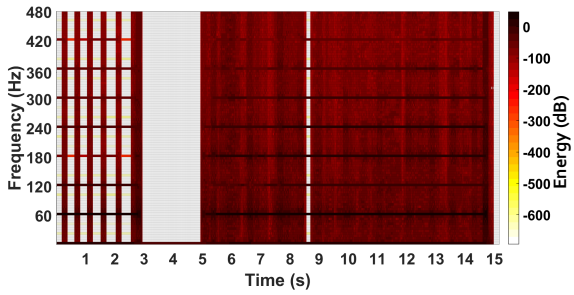


Fig. 3. Energy of current frequencies for gravel by FT.

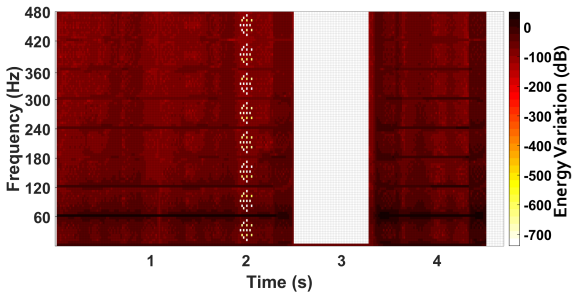


Fig. 4. Energy of current frequencies for grass by FT.

the average energy variation for each calculated WT resolution, where A represents the approximations and D the details. The higher the number following the identification letter, the higher the resolution level.

Depending on the signal sampling frequency, this behavior is more visible at certain levels of resolution. In this paper, as

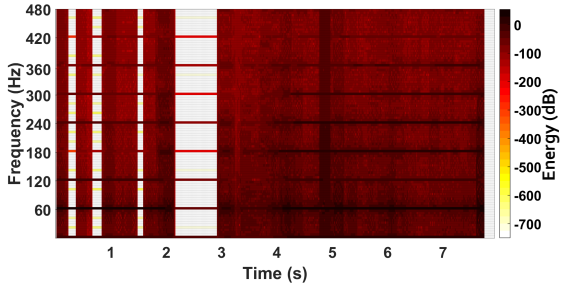


Fig. 5. Energy of current frequencies for clay by FT.

shown in Table II, there is a large average energy variation between cycles, but this variation is different between resolu-

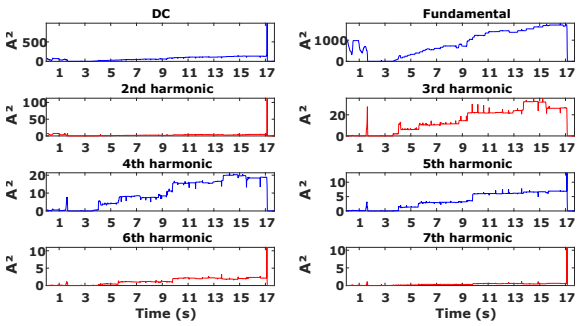


Fig. 6. Energy of the HIF current harmonic components calculated by the ST for sandy soil.

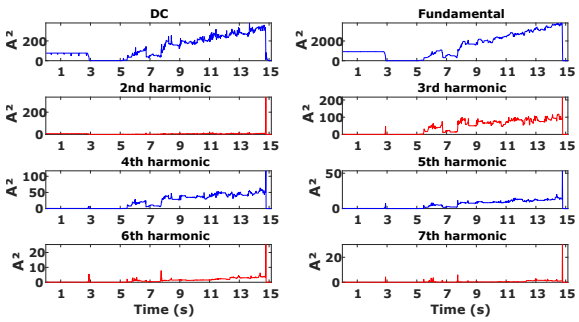


Fig. 7. Energy of the HIF current harmonic components calculated by the ST for gravel.

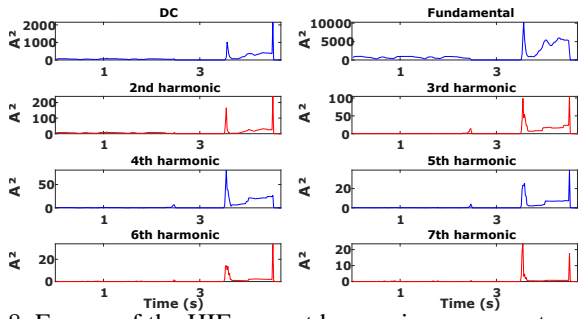


Fig. 8. Energy of the HIF current harmonic components calculated by the ST for grass.

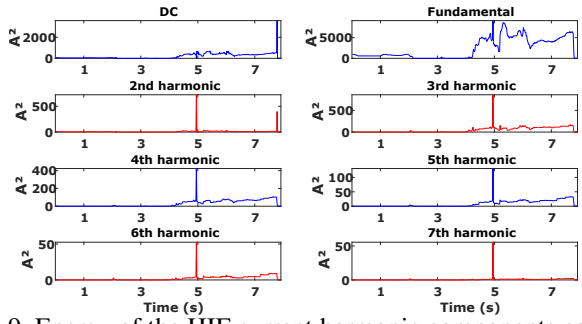


Fig. 9. Energy of the HIF current harmonic components calculated by the ST for clay.

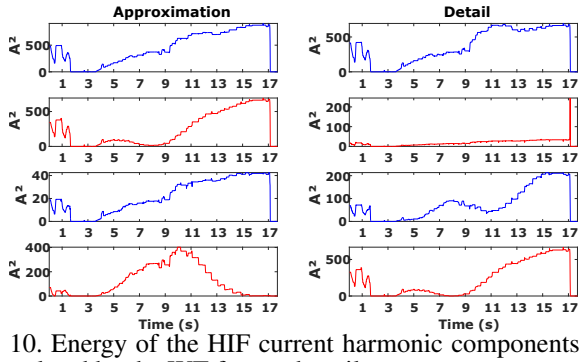


Fig. 10. Energy of the HIF current harmonic components calculated by the WT for sandy soil.

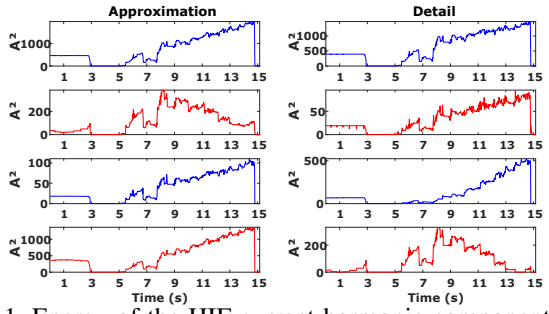


Fig. 11. Energy of the HIF current harmonic components calculated by the WT for gravel.

**Table** 1. **Average energy variation per ST ($A^2$).**

| Soil | Fund | $2^{nd}$ | $3^{rd}$ | $4^{th}$ | $5^{th}$ | $6^{th}$ | $7^{th}$ | $8^{th}$ |
|---|---|---|---|---|---|---|---|---|
| Sand | 6 | 0.3 | 0.4 | 0.20 | 0.08 | 0.05 | 0.04 | 0.04 |
| Gravel | 50 | 2.5 | 5.2 | 2.22 | 0.68 | 0.28 | 0.24 | 0.33 |
| Grass | 521 | 10 | 5.1 | 3.01 | 1.44 | 1.14 | 1.08 | 1.11 |
| Clay | 274 | 11 | 14.3 | 6.02 | 1.89 | 0.81 | 0.65 | 0.74 |

tion levels and among soils. This should be considered when applying WT in HIF studies. In Table II, the letter A represent the approximation resolutions and D, the details. The numbers 1, 2, 3 and 4 mean the level of the resolution.

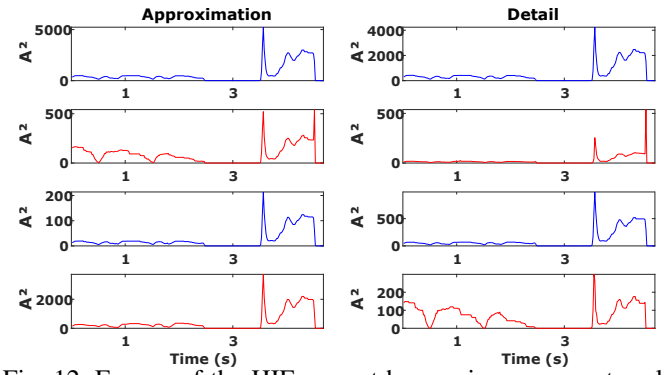


Fig. 12. Energy of the HIF current harmonic components calculated by the WT for grass.

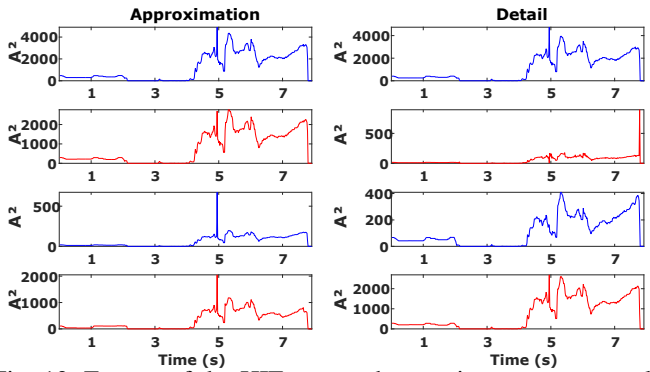


Fig. 13. Energy of the HIF current harmonic components calculated by the WT for clay.

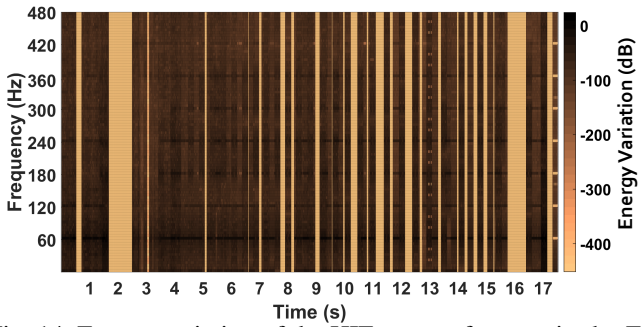


Fig. 14. Energy variation of the HIF current frequencies by FT for sandy soil.

**Table** 2. **Average energy variation by WT ($A^2$).**

| Soil | A1 | A2 | A3 | A4 | D1 | D2 | D3 | D4 |
|---|---|---|---|---|---|---|---|---|
| Sand | 3 | 3 | 2 | 1 | 0.25 | 1 | 2 | 2 |
| Gravel | 26 | 23 | 8 | 3 | 2 | 6 | 18 | 7 |
| Grass | 253 | 207 | 29 | 18 | 10 | 46 | 188 | 17 |
| Clay | 138 | 128 | 84 | 13 | 11 | 11 | 47 | 83 |

The three signal processing tools investigated showed potential ability to detect HIFs. Studies with the HIF-related interharmonics has promising results, as well as the frequency bands studies. Table I and Table II present the energy average during the electric arc, calculated by WT and ST. The results showed that for the soils of grass and clay, the average energy variation between cycles presented the highest values. The sandy soil showed the smallest energy variation by the calculation of the two transforms. It is important to notice that the WT has a wide variety of frequency bands and mother-wavelets that can be used, showing that it is more flexible to select the parameters, unlike FT and ST. On the other hand, it is noteworthy that WT and ST provide signal information at each sample, showing faster variations, unlike FT, which considers the signal station-

ary inside the window, and it may give inconclusive results to identify HIFs.

## 5. CONCLUSION

In this paper relevant characteristics of HIF currents for different types of soils were highlighted and discussed. It was shown that the energy variation values resulting from ST, FT and WT are strongly linked to the arc existence. Therefore, this characteristic can be used for HIF detection. Also, interharmonics were always present in the frequency spectrum calculated by FT. One big challenge is to define proper thresholds for HIF detection, since a wide range could be observed either for energy or for interharmonic amplitude. Moreover, a reliable HIF detection method must be immune against common transients and expected harmonic contents in PDS. In this way, the combination of two or more signal processing techniques can be investigated for composing HIF detection methods. With the development of smart grids and technologies, innovative equipment has become more practical in applications with higher data acquisition rates, for example, making it possible to observe higher frequency values of the signals in real time, with a high quality of data acquisition, as observed with the use of PLC.

## ACKNOWLEDGMENT

This work is supported by Grant 2018/14242-0 from São Paulo Research Foundation (FAPESP). Also, thanks to the authors of Carvalho et al. (2015), from Federal University of Uberlândia, for providing the HIFs data.

## REFERENCES

Belka, H. and Michalik, M. (2004). Application of The Continuous Wavelet Transform to Intermittent High Impedance Ground Fault Detection in MV Networks. In *Eighth IEE International Conference on Developments in Power System Protection*, 473–476.

Carvalho, D., Macedo, J.R., Resende, J.W., Castro, F.C., and Bissochi, C.A. (2015). Proposition of an interharmonic-based methodology for high-impedance fault detection in distribution systems. *IET Generation, Transmission & Distribution*, 9(16), 2593–2601.

Gomes, D.P.S., Ozansoy, C., and Ulhaq, A. (2018). High-sensitivity vegetation high-impedance fault detection based on signal's high-frequency contents. 33(3), 1398–1407.

Milioudis, A.N., Andreou, G.T., and Labridis, D.P. (2012). Enhanced Protection Scheme for Smart Grids Using Power Line Communications Techniques—Part I: Detection of High Impedance Fault Occurrence. *IEEE Transactions on Smart Grid*, 3(4), 1621–1630.

Mohamad, N.Z. and Abidin, A.F. (2012). S-transform based technique to detect high resistance symmetrical fault during power swing. In *2012 IEEE 8th International Colloquium on Signal Processing and its Applications*, 282–286.

Nam, S.R., Park, J.K., Kang, Y.C., and Kim, T.H. (2001). A modeling method of a high impedance fault in a distribution system using two series time-varying resistances in emtp. In *2001 Power Engineering Society Summer Meeting. Conference Proceedings*, volume 2, 1175–1180 vol.2.

Nason, G., Sapatinas, A., and Sawczenko, A. (2001). Wavelet Packet Modelling of Infant Sleep State Using Heart Rate Data. *Sankhya: The Indian Journal of Statistics*, 63(2), 199–217.

Routray, P., Mishra, M., and Rout, P.K. (2015). High impedance fault detection in radial distribution system using s-transform and neural network. In *2015 IEEE Power, Communication and Information Technology Conference (PCITC)*, 545–551.

Samantaray, S.R., Panigrahi, B.K., and Dash, P.K. (2008). High impedance fault detection in power distribution networks using time-frequency transform and probabilistic neural network. *IET Generation, Transmission & Distribution*, 2(2), 261–270.

Santos, W.C., Lopes, F.V., Brito, N.S.D., and Souza, B.A. (2017). High-impedance fault identification on distribution networks. 32(1), 23–32.

Stockwell, R.G., Mansinha, L., and Lowe, R.P. (1996). Localization of the complex spectrum: the s transform. 44(4), 998–1001.

Wang, X., Geng, J., and Dong, X. (2018). High-Impedance Fault Detection Based on Nonlinear Voltage–Current Characteristic Profile Identification. *IEEE Transactions on Smart Grid*, 9(4), 3783–3791.